Simulation Analysis of Magnetic Wheel Characteristics of Climbing Robot

Rui Chang

School of Mechanical and Transportation Engineering, China University of Petroleum (Beijing), Beijing 102249, China

2017214521@student.cup.edu.cn

Keywords: Wall-climbing robot, magnetic wheel, Magnetic field simulation

Abstract: Aiming at the permanent magnet wheeled wall-climbing robot, this paper proposes a permanent magnet wheel design scheme, and uses Maxwell to simulate the magnetic field distribution and magnetic adsorption force when using different materials for the magnetic wheel component. It can be seen from the simulation results that the magnetic adsorption force can be greatly improved by selecting suitable materials. When the inner and outer end caps of the magnetic wheel are made of a magnetic conductive material, the spacers and the support ring are non-magnetic materials, the average adsorption force is 234.63 N, which is 2.93 times when the inner and outer end caps, the spacers and the support ring are all magnetic materials.

1. Introduction

Wall-climbing robots are special robots that have been widely used in the fields of maintenance, construction, inspection and safety in the world. The wall-climbing robots can often be seen in the non-destructive testing of oil tanks [1, 2]. The adsorption mode can be roughly divided into negative pressure adsorption, magnetic adsorption and biomimetic adsorption. Among them, permanent magnet adsorption is widely used as a reliable adsorption method for steel walls [3].In this paper, a permanent magnet adsorption wheeled wall-climbing robot for non-destructive testing of tank surface is designed and its magnetic wheel characteristics are studied and analyzed.

2. Design of Permanent Magnet Wheel Climbing Robot

The structure of the robot consists of the adsorption module, the drive module, the control module, the power supply and the frame. In order to reduce the weight of the robot body, the frame is completely made of aluminum profiles. The connection force of the robot is completely provided by four magnetic wheels; the drive module uses a high torque DC motor; the control box and the power supply are mounted on the frame.

The structure of the magnetic wheel is shown in Fig. 1 (the joints such as studs and nuts are not shown in the figure), and the core part consists of three tile magnets and three spacers. Since the magnetic wheel requires a through hole when assembling, and the annular permanent magnet block is difficult to be processed again because of the material being brittle, the three spacers are used to separate the three tile-shaped permanent magnets. The through holes are machined on the spacers, and the spacers are bonded to the magnetic blocks using a stable adhesive. The ring has a support ring to support the annular structure composed of the magnetic block and the spacer. Use the studs and nuts to connect the components of the magnet wheel into one. The outer side of the magnetic wheel is covered with rubber to increase its friction.
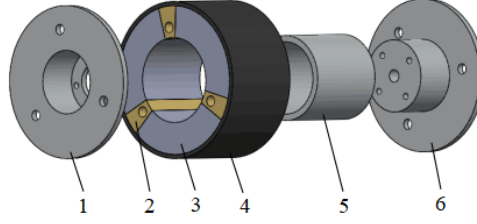
1—the outer end cap; 2—the spacer; 3—the magnet block;
4—rubber layer; 5—the support ring; 6—the inner end cap.

Fig. 1 Schematic diagram of magnetic wheel structure

3. Simulation Analysis of Magnetic Field and Magnetic Adsorption Force of Magnetic Wheel

3.1 Theoretical Basis of Finite Element Analysis

In the case where the material in the entire solution domain is isotropic, the expansion of Maxwell's equations in the three-dimensional coordinate system is [4]:

$$\begin{cases} \dfrac{\partial}{\partial y}\left(\dfrac{1}{\mu}\right)\boldsymbol{B}_z - \dfrac{\partial}{\partial z}\left(\dfrac{1}{\mu}\right)\boldsymbol{B}_y - \dfrac{1}{\mu}\left(\nabla^2\boldsymbol{A}\right)_x = 0 \\[2mm] \dfrac{\partial}{\partial z}\left(\dfrac{1}{\mu}\right)\boldsymbol{B}_x - \dfrac{\partial}{\partial x}\left(\dfrac{1}{\mu}\right)\boldsymbol{B}_z - \dfrac{1}{\mu}\left(\nabla^2\boldsymbol{A}\right)_y = 0 \\[2mm] \dfrac{\partial}{\partial x}\left(\dfrac{1}{\mu}\right)\boldsymbol{B}_y - \dfrac{\partial}{\partial y}\left(\dfrac{1}{\mu}\right)\boldsymbol{B}_x - \dfrac{1}{\mu}\left(\nabla^2\boldsymbol{A}\right)_z = 0 \end{cases} \tag{1}$$

$$\begin{cases} \left(\nabla^2\boldsymbol{A}\right)_x = \dfrac{\partial^2\boldsymbol{A}_x}{\partial x^2} + \dfrac{\partial^2\boldsymbol{A}_x}{\partial y^2} + \dfrac{\partial^2\boldsymbol{A}_x}{\partial z^2} \\[2mm] \left(\nabla^2\boldsymbol{A}\right)_y = \dfrac{\partial^2\boldsymbol{A}_y}{\partial x^2} + \dfrac{\partial^2\boldsymbol{A}_y}{\partial y^2} + \dfrac{\partial^2\boldsymbol{A}_y}{\partial z^2} \\[2mm] \left(\nabla^2\boldsymbol{A}\right)_z = \dfrac{\partial^2\boldsymbol{A}_z}{\partial x^2} + \dfrac{\partial^2\boldsymbol{A}_z}{\partial y^2} + \dfrac{\partial^2\boldsymbol{A}_z}{\partial z^2} \end{cases} \tag{2}$$

In the formula (1, 2), A is a magnetic field strength, and B is a magnetic induction intensity. The adsorption force can be calculated by the formula (1, 2) in combination with the magnetic field boundary conditions.

According to the Maxwell stress-tension method, the adsorption force of a permanent magnet unit is:

$$F = \oint_S \boldsymbol{T}dS = \oint_S \left[\frac{1}{\mu}(\boldsymbol{B}\bullet\boldsymbol{n})\boldsymbol{B} - \frac{1}{2\mu}\boldsymbol{B}^2\boldsymbol{n}\right]dS \tag{3}$$

In the formula (3), S is a closed curved surface in a uniform and isotropic medium; n is a unit vector of the outer normal of the microelement dS; B is a magnetic flux density; and μ is a relative magnetic permeability.

3.2 Magnetic field simulation analysis

The magnetic blocks of the magnetic wheel are axially magnetized, and the magnetization directions of the three magnetic blocks are the same. The tile-shaped permanent magnet has a width of 40 mm, an inner diameter of 40 mm, an outer diameter of 70 mm, a central angle of 102°, and a material of N35 NdFeB permanent magnet. The width and inner and outer diameter of the spacer are

the same as the magnet, and the central angle is 18°. The outer diameter of the support ring is 40 mm, the inner diameter is 34 mm, and the length is 40 mm. The outer rubber layer of the permanent magnet has a thickness of 2 mm.

Consider the following four cases:

Case1.The spacers, the support ring, and the inner and outer end caps are all magnetic conductive materials (In this paper, the magnetic materials are all made of steel graded steel-1008).

Case2.The spacers, the support ring and the inner and outer end caps are non-magnetic materials (The non-magnetic materials in this paper are all alumina).

Case3.Spacers are magnetically permeable material, and the support ring and the inner and outer end caps are non-magnetic materials.

Case4.The inner and outer end caps are magnetically permeable, and spacers and support ring are non-magnetic materials.

The magnetic field distribution of the magnetic wheel is simulated in the above four cases, and the simulation results are shown in Fig. 2-5.
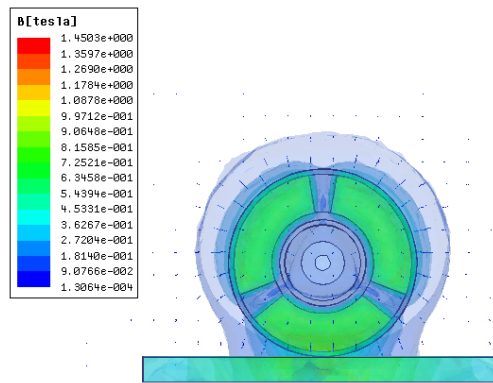
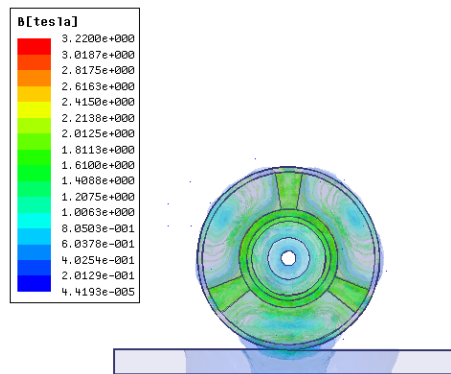

Fig. 2 Magnetic field distribution of case1

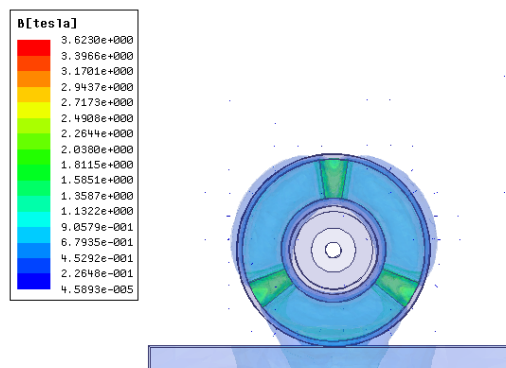Fig. 3 magnetic field distribution of case2
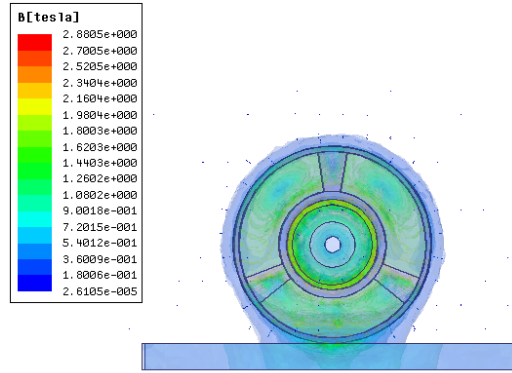

Fig. 4 Magnetic field distribution of case3

Fig. 5 Magnetic field distribution of case4

As can be seen from the figures, the magnetic field distribution of the magnetic wheel of Case 1 is the most compact, and the magnetic field distribution of the magnetic wheel of Case 2 is the most divergent. The main cause of this phenomenon is that the high magnetic permeability material has low magnetoresistance characteristics. When the spacers, the support ring, and the inner and outer end caps are all magnetically permeable materials, the magnetic field will pass through the magnetically permeable material with little magnetic reluctance and will not diffuse into the surrounding space, so the magnetic field is most concentrated.

The magnetic attraction force is the largest when the distance between the magnet block and the wall surface is the closest, as shown in Fig. 6; and is the smallest when the spacer block is closest to the wall surface, as shown in Fig. 7. The maximum adsorption force and the minimum adsorption force of the cases 1 to 4 were simulated and calculated, and the results obtained are shown in Table 1.
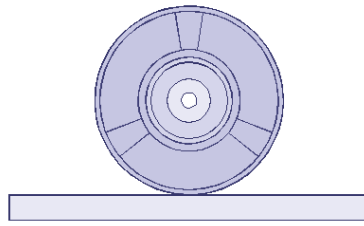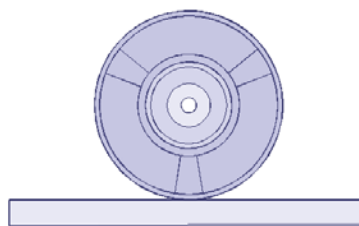

Fig. 6 Position 1   Fig. 7 Position 2

Table. 1 Four Cases comparing

Force/N	Case 1	Case 2	Case 3	Case 4
Maximum adsorption force	107.89	157.92	113.52	251.26
Minimum adsorption force	52.35	122.58	65.48	217.99
Average adsorption force	80.12	140.25	89.5	234.63
Difference	55.54	35.34	48.04	33.27

It can be seen from Table 1 that when the spacer blocks, the support ring, the inner and outer end caps are all magnetic conductive materials, the magnetic wheel has the smallest adsorption force, and the difference between the maximum adsorption force and the minimum adsorption force is the largest; while when the spacer blocks and the support ring are non-magnetic materials, and the inner and outer end caps are magnetic conductive materials, the magnetic wheel has the largest adsorption force, and the difference between the maximum adsorption force and the minimum adsorption force is the smallest. The average adsorption force is the average of the maximum adsorption force and the minimum adsorption force. As can be seen from Table 1, the adsorption force of Case 4 is 2.93 times the average adsorption force of Case 1. Therefore, the selection of suitable materials can greatly increase the magnetic wheel adsorption force.

4. Conclusion

In this paper, a permanent magnet wheel design scheme is proposed, and the magnetic adsorption force is simulated and calculated when different materials are selected for the magnetic wheel components. It can be seen from the simulation results that the magnetic wheel has the largest adsorption force in case 4, which is 2.93 times that of case1. Therefore, the selection of suitable materials for the various components of the magnetic wheel can greatly improve the magnetic adsorption force. The material of each component of the magnetic wheel is finally determined as shown in case4.

References

[1] S. Park, H. D. Jeong, Z. S. Lim. Design of a mobile robot system for automatic integrity evaluation of large size reservoirs and pipelines in industrial fields: Proceedings 2003 IEEE/RSJ International Conference on Intelligent Robots and Systems [C]. Las Vegas, Neva, USA: IEEE, 2004.

[2] H. R. Choi, S. M. Ryew, T. H. Kang, J. H. Lee, H.M. Kim. A wall climbing robot with closed link mechanism: Proceedings 2000 IEEE/RSJ International Conference on Intelligent Robots and Systems [C].Takamatsu, Japan: IEEE, 2002.

[3] Manuel F. Silva, J. A. Tenreiro Machado et al. A Survey of Technologies for Climbing Robots Adhesion to Surfaces: IEEE 6th International Conference on Computational Cybernetics [C]. Slovakia: IEEE, 2008.

[4] YAN X K, XIE D X,GAO Z X,et al.Research on integration path selection of Maxwell stress tensor method used in electromagnetic force FEM analysis [J].Transactions of China Electrotechnical Society, 2003(05): 32-36.